CHEMISTRY OF MATERIALS
pubs.acs.org/cm Article

Comprehensive Study of the Chemical, Physical, and Structural Evolution of Molecular Layer Deposited Alucone Films during Thermal Processing

Vamseedhara Vemuri, Sean W. King, William A. Lanford, John T. Gaskins, Patrick Edward Hopkins, Jeremy Van Derslice, Han Li, and Nicholas C. Strandwitz*

Cite This: *Chem. Mater.* 2023, 35, 1916−1925

Read Online

ACCESS | Metrics & More | Article Recommendations | Supporting Information

ABSTRACT: Thermal processing of molecular layer deposited (MLD) hybrid inorganic−organic alucone thin films produced porous and low-*k* materials. Alucone films were deposited by MLD using trimethyl aluminum and ethylene glycol at 120 °C. Changes in the film density and thickness during annealing were monitored using *in-situ* X-ray reflectivity and were compared to atomic layer deposited (ALD) alumina films. The chemical evolution of the as-deposited and annealed alucone films during post-deposition heating with and without UV was probed using infrared spectroscopy, Rutherford backscattering, nuclear reaction analysis, and ^{15}N spectroscopy, providing a detailed understanding of the induced changes. The concentration of OH groups decreased after depositing 1 nm of alumina capping layer as a barrier to moisture uptake, which also decreased the etch rate in CF_4/O_2 plasma. The lowest dielectric constant of the processed alucone films (k_{min} = 4.75) was 25% lower than the lowest values measured in ALD alumina counterparts (k_{min} = 6.7). Large thickness decreases for alucone films were observed at ∼200 °C of anneal temperatures. Removal of retained organic components by thermal processing of MLD films is demonstrated to be a promising and versatile route to porous thin films for a wide range of applications including low dielectric constant materials.

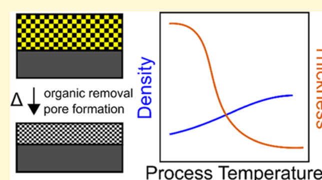

Downloaded via UNIV OF CALIFORNIA SANTA BARBARA on June 15, 2023 at 18:39:43 (UTC).
See https://pubs.acs.org/sharingguidelines for options on how to legitimately share published articles.

■ INTRODUCTION

Since the inception of integrated circuits, the areal density of components, such as transistors, has increased along with a decreasing component size with the aim of increasing computational speeds. Additional increases in computing speed can be achieved by the continued minimization of the resistance and capacitance delays that occur due to the resistivity of metal lines and the capacitance of dielectrics. As a historical example, aluminum was replaced with copper-reducing resistance delays by 36%.[1,2] Capacitance delays are introduced from the interlayer dielectric (ILD) and etch stop materials (ES) present in the backend of the line (BEOL) and are exacerbated by the close proximity of metal lines.[3] The capacitance can be decreased by decreasing the dielectric constant (k) of the ILD.[4] Hence, to decrease the net capacitance delays in BEOL, the k of the ES and ILD should be decreased. However, the mechanical and thermal properties of these layers are also important as they reinforce the metal lines to distribute the shear stress and dissipate thermal energy during processing, packaging, and operation.[5−8] Further, the etch behavior of ES and ILD films is also highly important for processing, in which case large differences in etch rates between the ILD and ES layers are generally desired.

Currently, a-SiC:H (k = 4−7),[8−14] a-SiCN:H (k = 4.5−5.8),[12,15−18] and a-SiN:H (k = 6.5−7)[19−21] are used as ES materials and their thermal conductivity, Young's modulus, etch rates, and dielectric constants vary based on their deposition and processing parameters. A desirable combination of material properties for new ES materials includes low-k values and low CF_4/O_2 plasma etch rates, high thermal conductivity, high indentation modulus, and low leakage current density, motivating the investigation of non-Si-based dielectrics.

The prospect of using alternative dielectrics, such as aluminum oxide, has merit due to their ease of deposition and different etch behaviors relative to Si-based dielectrics. Alumina deposited using atomic layer deposition (ALD) exhibits thermal conductivity values of 1.3−2.6 W/mK,[22−24] a high Young's modulus of 168−182 GPa,[25] a low CF_4/O_2 plasma etch rate of 0.5−1 nm/min (current study), and a dielectric constant of 7−8.5.[26−30] Most of these properties are generally favorable for ES layers; however, the dielectric constant of alumina is high compared to existing Si-based dielectrics. Thus, maintaining the other properties while reducing k values may enable a new material composition for ES and other dielectric layers without significant capacitance penalties.

Received: October 11, 2022
Revised: February 6, 2023
Published: February 22, 2023

© 2023 American Chemical Society

One strategy for decreasing k of a material is to incorporate organic molecules with low polarizability and/or to induce porosity. Porogen molecules can be subsequently removed by post-deposition thermal processing to introduce porosity. This strategy is employed for fabricating ultra-low-k SiCOH films.[31] For example, the growth of porous ultra-low-k SiOCH has been achieved using diethoxymethylsilane as a network-forming matrix precursor and α-terpinene as a sacrificial porogen. As-deposited films are subsequently annealed at temperatures near 385 °C for 2−4 h in broad-band UV light (200−400 nm) to remove the porogen leaving a porous SiOCH scaffold.[32] Another related and highly effective strategy for inducing porosity in inorganic solids is through the wet chemical combination and subsequent thermal processing of inorganic precursors and organic pore formers. Examples include the use of ionic or nonionic surfactants to template mesoporous solids.[33,34]

Molecular layer deposition (MLD) and the formation of so-called "metalcones" represent another strategy for the integration of organic molecules and inorganic structural units that may provide a path to porous dielectrics. The organic components in MLD may act as low dielectric constant components and/or as porogens, analogous to the organic molecules incorporated in SiCOH films and wet chemical routes described above. The focus materials of this study are Al-containing inorganic−organic hybrid materials (alucones)[35,36] that can be deposited using MLD and may provide a route to porous Al-based dielectrics with lower k values than nonporous aluminum oxide. Incorporation of organic components into the Al_2O_3 matrix decreases the mass density,[37] which may result in lower k values than Al_2O_3.

By subjecting the alucone films to post-deposition processing, such as annealing or air exposure, removal of organics and the formation of porosity have indeed been observed.[38,39] Calcination at 500 °C and etching with water removed the organics, and porosity was introduced in alucone films as evidenced by ellipsometric porosimetry.[40−43] The details of the chemical (e.g., compositional) and structural (e.g., density) evolution of alucone films during post-deposition heating, however, are not well understood. In addition, the moisture uptake of alucones can significantly modify film chemistry.[39] This moisture uptake has deleterious effects on dielectric and mechanical reliability of low-k films causing early breakdown.[44−46] Here, we report the deposition and characterization of MLD alucone films and examine the role of post-deposition annealing and the effects of short wavelength UV light irradiation on the physical, chemical, and electrical properties of the films. We addressed the stability issue of the alucone films by depositing a 1 nm alumina cap as a barrier to prevent water uptake and film degradation. This 1 nm alumina film acts as a barrier to moisture permeation in addition to decreasing the etch rate of alucone films in the dry plasma.

■ EXPERIMENTAL METHODS

The hybrid metalcone films were deposited using a custom-made viscous flow reactor with 6.35 cm inner diameter and 75.2 cm length following a previously reported system.[47,48] Research-grade N_2 (99.9999%, Praxair) was used as the carrier gas. A continuous flow of the carrier gas (60 sccm) under continuous pumping resulted in a pressure of ∼250 mTorr during the growth. The reactor was maintained at 120 °C, and the manifold, precursor delivery line, and the stop valve were heated to 150 °C.

Alucone films were deposited using trimethyl aluminum (TMA, 99%, STREM Chemicals) and ethylene glycol (EG, 99%, Sigma-Aldrich), and alumina films used for comparison were deposited using TMA and 18.2 MΩ of water. Unless specified, all of the metalcone samples used for various structural characterization were grown on ∼1.5 × 1.5 cm^2 test-grade (100) p-Si with a thin native oxide. The substrates were cleaned by sonicating in isopropanol and water prior to growth. The alucone films were grown using two 0.1 s TMA doses with a 5 s interval followed by two 0.6 s EG doses with a 5 s interval and a 60 s purge time in between TMA and EG doses.

A custom-built UV cure chamber utilized a 172 nm wavelength Xe-excimer lamp (Ushio) and a 15.2 × 10.2 cm^2 heated aluminum stage. The as-deposited films were annealed at 150, 250, or 350 °C for 10 min either with or without UV irradiation in an inert N_2 (99.999%; PRAXAIR) atmosphere where the base pressure of the chamber was 60 mTorr under constant pumping. The N_2 flow inside the reactor was controlled using a needle valve. Low-k SiCOH samples from Intel Corporation were used to test the UV cure chamber.

Film thickness was measured using spectroscopic ellipsometry (SE) using a J.A. Woollam VASE ellipsometer with incident angles 60 and 70° from 350 to 850 nm. The thickness of the samples was determined by fitting with a Cauchy model.

For measuring the electrical properties, metal-oxide-semiconductor capacitors (MOSCAPs) were fabricated by depositing alucone films on (100) p-Si with resistivity 1−10 Ω-cm. The silicon wafers were cleaved to 1.5 × 1.5 cm^2 pieces and were cleaned by sonicating in isopropanol (IPA) and water and then subjected to Radio Corporation of America (RCA) cleaning 1 and 2.[49] After RCA cleaning, the samples were hydrogen-terminated by immersion in 5% hydrofluoric acid (Transene, Inc.) for 1 min followed by rinsing with water and drying under a filtered N_2 (g) stream.

Capacitance−voltage measurements used a HP4194A impedance analyzer and mercury probe (MDC 802B). The mercury drop from the probe was the front contact, and a silver paste was scratched on the backside to attach an aluminum plate to make an ohmic backcontact. The mercury drop area was calculated before every measurement from a thermal oxide-coated Si calibration sample, and some low-k SiCOH samples from Intel Corporation were used for calibration. The dielectric constant of the MOSCAP test structures was extracted using $C = \frac{k\varepsilon_0 A}{t}$, where C is the capacitance of the film, k is the dielectric constant, ε_0 is the permittivity of free space, A is the area of the mercury drop, and t is the thickness of the film.

FTIR spectra were obtained by depositing films on a 2 × 6.5 cm^2 double-side polished (DSP) float zone Si(100) (Virginia Semiconductor) or DSP test-grade Si wafer (University Wafer). The DSP Si wafers were cleaned by sonicating sequentially in IPA and 18.2 MΩ of water followed by a 5 min UV ozone cleaning. FTIR measurements were performed in transmission mode using a Perkin Elmer Spectrum 100 with N_2 purge. The FTIR background spectrum was collected from the substrate after cleaning but prior to film growth to isolate the signal from the film. The spectra were collected from 750 to 4000 cm^{-1} and averaged over 250 scans using a resolution of 4 cm^{-1}.

X-ray reflectivity (XRR) measurements used a PANalytical Empyrean X-ray diffractometer with Cu X-ray tube with a wavelength of 1.54 Å. The *in-situ* XRR measurements used a DHS 1100 (Anton Paar) heating stage in air from 50 to 800 °C at 50 °C intervals. The XRR data were fit for density and thickness using X'pert reflectivity software. *In-situ* XRR data were obtained from alucone films deposited on 1.5 × 1.5 cm^2 thermal oxide (500 nm) Si substrates to avoid the growth of interfacial oxide (SiO_2) during heating, whereas the *ex-situ* experiments are performed on 1.5 × 1.5 cm^2 test-grade (100) p-Si with a thin native oxide.

The composition analysis used several techniques including ^{15}N nuclear reaction analysis (NRA, for H), 1.2 MeV deuteron (D, for C, O) NRA, and 2 MeV He Rutherford backscattering analysis (RBS, for Al). This combination of analysis techniques was used to measure the concentration of lighter elements including H and heavier elements C, O, and Al present in alucone films. The measurements were performed at the University of Albany, and the experimental

procedure can be found elsewhere.[50] A Ni thin film of ∼100 nm was deposited on the Si wafer using electron beam evaporation prior to alucone deposition to differentiate between the signals of Si and Al due to their close atomic number.

The thermal conductivity of the alucone films was measured using steady-state thermoreflectance (SSTR).[51] In this technique, a pump laser was used to heat the surface of the samples, coated in 80 nm of aluminum, and a probe laser measured the changes in reflectivity, related to temperature, due to incrementally increasing the input pump laser power. The relationship between the input pump power and the resulting change in reflectivity is used to determine the thermal conductivity of the alucone films.

Ellipsometric porosimetry probed the volume of open porosity in the as-deposited and annealed alucone samples. The samples were heated in vacuum to 100 °C for 10−20 min prior to the measurements to remove the adsorbed water. Initially, water and toluene were used to perform the adsorption−desorption measurements on the as-deposited sample and the hysteresis behavior observed was nonreversible. IPA was found to be more reliable and was used to perform all of the subsequent measurements.[52]

The indentation modulus of the films was determined by nanoindentation using a Berkovich cube corner diamond tip and Hysitron tribo indenter.[53] Ten measurements at different locations were acquired.

Etching of the hafnia and hafnicone samples in CF_4/O_2 plasma was done using a Technics MICRO-RIE series 800 tool. The gas used was 96% CF_4 and 4% oxygen mixture. The conditions were 250 W power, and the gas flow was set to maintain a base pressure of 200 mTorr. The samples were etched for 2 min, and the etch rate was calculated by measuring the thickness after etch using the spectroscopic ellipsometry.

■ RESULTS AND DISCUSSION

The density and thickness evolution of alucone and alumina control films with thermal processing were probed using *in-situ* X-ray reflectivity (XRR) measurements from 50 to 800 °C at 50 °C intervals in air (Figure 1). The density of alumina increased by ∼4%, whereas the density of alucone increased by 24% from 50 to 800 °C. Throughout the entire temperature range examined, the density of the alucone films was significantly lower than those of ALD alumina samples. The thickness of alumina decreased by 5% during heating to 800 °C, whereas the thickness of alucone decreased by 74%. A decrease in alucone film thickness of ∼4% was observed at 100 °C, indicating instability even at or below film growth temperatures (here, 120 °C). Notably, up to 250 °C, the alucone films remained at near-constant density despite large decreases in thickness, indicating that mass loss was somewhat balanced with thickness decreases. When organic polymers are annealed above 200 °C, volatile products such as CO, CO_2, and CH_4 are evolved accompanied by mass loss, likely due to the cleavage of C−C and C−H bonds.[54,55] The observed thickness decrease in the 200−400 °C range in alucone films can thus likely be attributed to mass loss due to the cleavage of C−C, C−H bonds, and/or the desorption and removal of EG species. The cleavage of C−C and C−H bonds and the release of the volatile products lead to the formation of reactive free radicals in the films.[56,57] When the films are annealed above 500 °C, the reactive free radicals form polyaromatic ring structures, which undergo condensation to release H_2.[38] Thus, the decrease in thickness observed from 550 to 600 °C could be attributed to the condensation of the polyaromatic ring structures. The decrease in thickness and increase in density for the ALD alumina films can be attributed to dehydration and dehydroxylation through condensation and loss of water.[58] For the alucone films, along with dehydration, the loss of mass

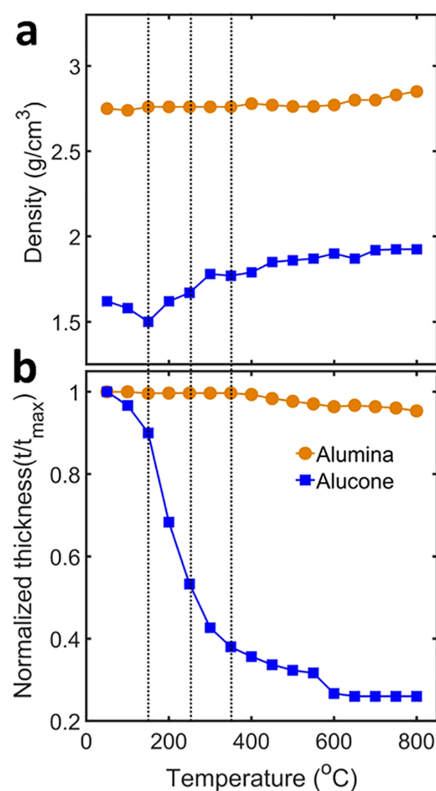

Figure 1. (a) Density vs temperature and (b) normalized thickness vs temperature for alumina and alucone films fit from the *in-situ* temperature-dependent XRR. The vertical dotted lines represent the temperatures at which the *ex-situ* measurements were conducted.

due to removal of organics and collapse of the remaining structure likely plays a major role in the thickness decrease.

The density evolution of the alumina and alucone films after thermally processing from 150 to 350 °C at 100 °C intervals in both the presence and absence of UV light in N_2 ambient was also probed using *ex-situ* heating and subsequent XRR to elucidate the role of short wavelength (172 nm) UV on the annealing process (Figure S3).[59−61] The density of the alucone films increased with annealing temperature similar to the *in-situ* experiment in air, although slightly higher densities were measured in the *ex-situ* processed samples. These slight differences may be ascribed to the different heating rate and ambient atmosphere between the measurements. The density of the alucone samples annealed in UV was ∼3−9% larger than that of the corresponding samples annealed without UV at the same anneal temperature, indicating that annealing in UV may induce additional densification, although this effect is small.

FTIR measurements were conducted to examine the chemical evolution of the alucone films after thermal processing with and without UV exposure (Figure 2). The broad peak observed in the range of 3000−3650 cm^{-1} is ascribed to −OH species, indicating the presence of adsorbed water and/or hydroxyl species within the films. The peak observed at 1615 cm^{-1} can be partially attributed to the scissor mode of adsorbed water.[62] The peaks observed at 1615 and 1415 cm^{-1} may correspond to enolate-type vinyl ether species, C=C and $=CH_2$, respectively.[63] The enolate-type vinyl ether and the −OH species may arise from alumina-catalyzing HO−CH_2−CH_2−O−Al species to enol ether (CH_2=CH−O−Al), vinyl ether (HO−CH=CH−O−Al) species, H_2, and H_2O.[36,64,65] The peaks observed at 2942 and 2879 cm^{-1}

https://doi.org/10.1021/acs.chemmater.2c03107
Chem. Mater. 2023, 35, 1916−1925

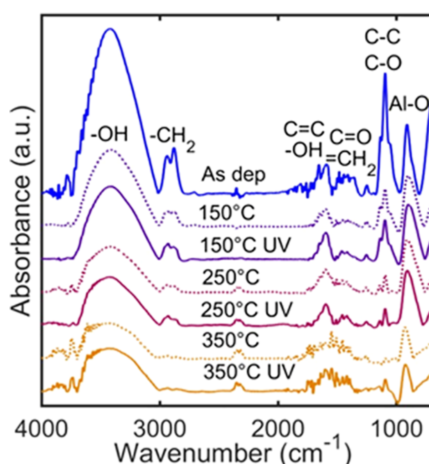

Figure 2. FTIR spectra of alucone films measured after thermal processing including assignments of various species.

correspond to the asymmetric and symmetric stretching vibrations of $-CH_2$ species. The peaks observed at 1132 and 1086 cm^{-1} represent the C−C and C−O vibrations. These features indicate the presence of ethylene glycol in the films. The peaks at 905 cm^{-1} are ascribed to the Al−O stretching vibrations.[66−68]

The absorbance intensity of the −OH (3000−3650 and 1615 cm^{-1}), $-CH_2$ (2942, 2879 cm^{-1}), and C−C/C−O (1132, 1086 cm^{-1}) decreased, and the peak at 3800 cm^{-1} disappeared after annealing at 150 °C. This decrease in intensity indicates the partial removal of water and/or hydroxyls and organics from the film. After annealing the film at 250 °C, further decrease in the absorbance intensity of −OH, CH_2, and C−C/C−O was observed, corresponding to further removal of absorbed water and organics from the film. A red shift and decrease in intensity of the −OH peak corresponding to the changes in the bonding of hydroxyl species present inside the film were also observed. The peak near 3800 cm^{-1} reappears, which corresponds to surface hydroxyls. The intensity of the Al−O peak (905 cm^{-1}) decreases after processing the films at 350 °C.

Considering just the effect of UV during the annealing process, the UV exposure did not cause any significant changes in the FTIR spectra of the films relative to the UV-free anneal. The *ex-situ* XRR-derived density (Figure S1) indicated that annealing alucone in UV caused slightly more densification than only annealed samples. For comparison, in SiCOH films grown using plasma-enhanced chemical vapor deposition, annealing in UV causes structural changes such as a Si−O network to cage Si−O−Si transition and chemical changes that correspond to the removal of organics seen by decreases in CH_x and Si-CH_3 peaks.[59] Thus, significant differences were not observed with and without UV exposure during the annealing (or curing) of alucone films unlike in UV processed relative to SiCOH films. These differences could be due to the different behaviors of these Al-based films or different intensities/wavelengths of UV light used in this study.

To better understand the evolution of the −OH stretching region (3000−3800 cm^{-1}) from Figure 2, the FTIR spectra from as-deposited and thermally processed films are deconvoluted into three different components that are attributed to the (Al−OH)−(Al−OH) species connected via H bonding (3400 cm^{-1}), isolated Al−OH species (3650 cm^{-1}), ice-like water (3230 cm^{-1}), and surface hydroxyl species (3800 cm^{-1}) (Figure 3a,b).[69−71] The integrated absorbance of the species assigned to (Al−OH)−(Al−OH)

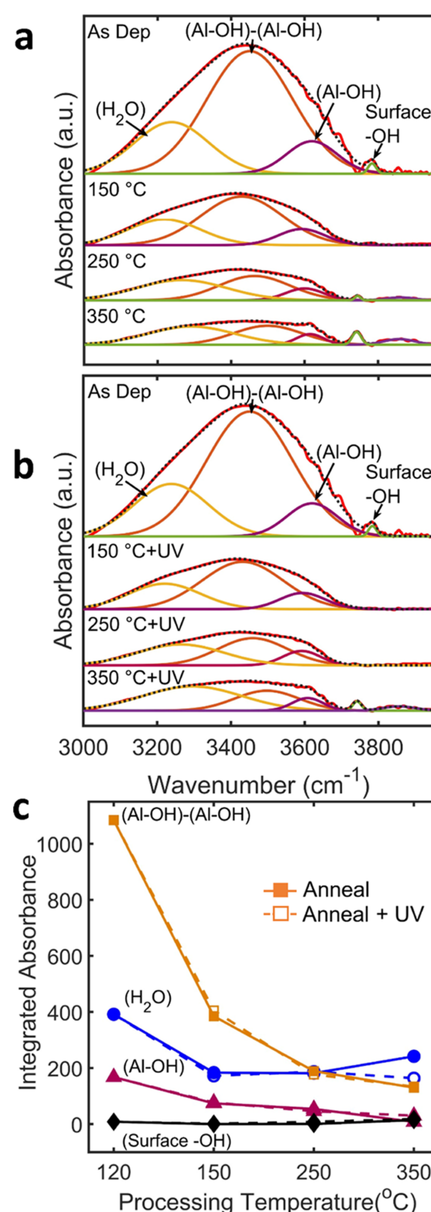

Figure 3. (a) *Ex-situ* FTIR spectra of as-deposited and processed alucone films (a) without and (b) with the presence of UV during annealing. (c) Integrated absorbance of regions assigned to (Al−OH)−(Al−OH) (3400 cm^{-1}), H_2O (ice-like water (3230 cm^{-1})), isolated Al−OH (3650 cm^{-1}), and surface −OH (3800 cm^{-1}).

and Al−OH decreased with annealing, whereas the intensity of the free H_2O and surface hydroxyls decreased until 250 °C and then increased after 350 °C anneal (Figure 3c). The major decrease (around 92%) in the intensity was seen for H-bonded (Al−OH)−(Al−OH) and may be due to dehydroxylation and condensation resulting in Al−O−Al bonding. A 50% decrease in the integrated absorbance of the component assigned to water after annealing the films at 350 °C was observed, indicating that a significant fraction of water is retained in the films after this annealing step. The signature of free Al−OH species approaches zero after annealing at 350 °C. The weak

https://doi.org/10.1021/acs.chemmater.2c03107
Chem. Mater. 2023, 35, 1916−1925

surface hydroxyl species signature disappeared after annealing at 150 °C but reappeared after 350 °C anneal.

Possible porosity in the thermally processed and as-deposited alucone films and the hydrophilicity of the internal surfaces renders the films susceptible to the uptake of H_2O from ambient air, which can cause chemical changes and increase k values.[43] In an effort to prevent moisture uptake, ALD alumina capping layers (10 ALD alumina cycles, nominally 1 nm) were deposited immediately after post-deposition thermal processing on an additional set of samples. We chose to explore this strategy to prevent water uptake because ALD alumina has been used as a barrier previously to prevent moisture diffusion from atmosphere.[72] Changes in the FTIR spectra induced by this ALD step are shown in Figure 4.

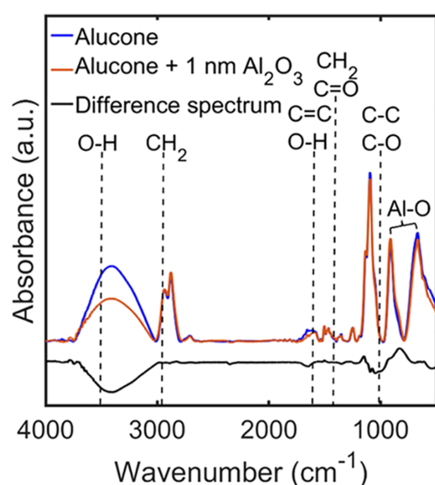

Figure 4. *Ex-situ* FTIR spectra of as-deposited alucone, alucone with ALD cycles of Al_2O_3, and difference spectrum.

A decrease in the intensity of the O−H stretching peak (3000−3800 cm^{-1}) was observed indicating the removal or reaction of water or OH groups. The difference spectrum also shows negative peaks near 1600 cm^{-1} (adsorbed H_2O) and around 1000 cm^{-1} (C−C and C−O) indicating the removal of some absorbed water and organics. There is a slight increase in the intensity of the Al−O peak around 905 cm^{-1} indicative of the expected increase in the quantity of Al−O bonding. Since TMA is known to diffuse into some films during growth,[73] the physisorbed water might react with TMA forming alumina domains inside the film rather than just on the top surface.

RBS, NRA, and ^{15}N spectroscopies were used to determine the elemental composition of the as-deposited and annealed alucone films that included 10 cycles of ALD alumina as a capping layer. The elemental compositions are represented per volume by accounting for the thickness (measured by SE) of each sample (Figure 5a) and together are used to calculate the mass density, which is compared to the XRR-derived mass density (Figure 5b). The concentrations of H and C decreased with increasing annealing temperature, confirming the removal of organics. The concentration of Al and O increased with increasing annealing temperature due to the decrease in film thickness and the increase in film density.

Annealing increased the density of the alucone films, and the samples annealed in the presence of UV light attained a larger mass density relative to the purely annealed analogues. This trend was observed independently by RBS/NRA and *ex-situ* XRR, although in some cases the differences are likely not

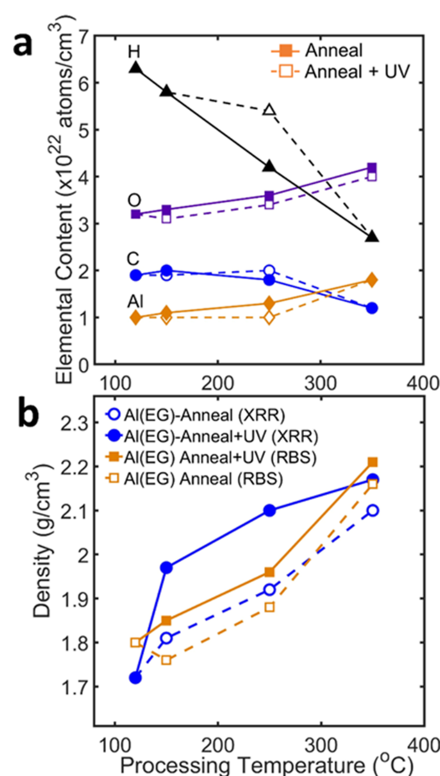

Figure 5. (a) Elemental composition of as-deposited (120 °C) and thermally processed films with an alumina (1 nm) capping layer, measured by using RBS and NRA spectroscopies, and (b) comparison of densities measured using XRR and RBS/NRA.

significant (Figure 5b). Despite differences in density probed using RBS and *ex-situ* XRR, both techniques show a similar trend in the density increase with increase in processing temperature corresponding to the removal of organics and water and a decrease in thickness. Differences in the density derived from XRR and RBS/NRA may be ascribed to differences in the measurement techniques and the fact that samples used for RBS/NRA had a 1 nm alumina capping layer, whereas the XRR samples did not. RBS/NRA provides the total areal density of a given atom in the film and thus provides an average density over the entire film, whereas XRR utilizes the critical angle of X-ray reflection, thus probing the film density near the air/film interface. Thus, the XRR and RBS/NRA densities may not agree if the density of the film is nonuniform. No attempts were made to fit multilayer films or film density gradients.

The dielectric constant (k) is an important property of dielectric materials for applications in microelectronics and was quantified here by the measurement of MOS capacitors where the dielectric layer consisted of alumina, alucone, or alucone with 10 ALD alumina cycles (Figure 6). The dielectric constant of alumina is generally larger than all of the alucone samples measured except for the as-deposited alucone film without the capping layer. The dielectric constant of the as-deposited alucone films was comparable to that of the as-deposited alumina films, which may be attributed to water or hydroxyl species within the film, as evidenced by FTIR (Figure 2). Since the k of water is 80, moisture uptake in a material can significantly increase the dielectric constant.[74] The dielectric constant of the alucone films decreased with increasing annealing temperature, which may be attributed to the

https://doi.org/10.1021/acs.chemmater.2c03107
Chem. Mater. 2023, 35, 1916−1925

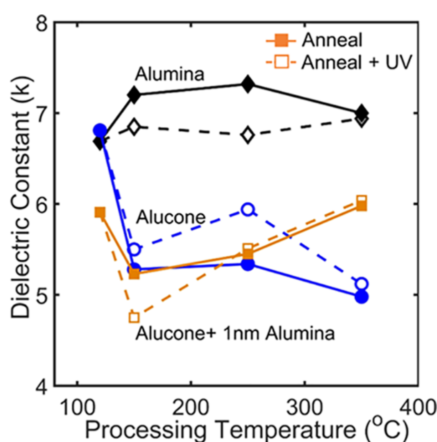

Figure 6. Dielectric constant evolution of the as-deposited (120 °C) and annealed alumina, alucone, and alucone with 10 cycles of alumina films.

decrease in the concentration of absorbed water that was also evidenced in FTIR data and/or the formation of porosity. The dielectric constant of the as-deposited alucone films decreased after depositing 10 cycles of alumina as a barrier. While the deposition of (relatively high *k*) ALD alumina alone would be expected to increase the film permittivity, the decrease may be due to the removal of OH/H_2O within the film as indicated by the decrease in the IR absorbance feature in the OH/H_2O region (Figure 4). The low-*k* values of the alucone-derived films further support the presence of porosity in these films and their potential for use as low-*k* materials not based on silicon.

The thermal conductivity of the alucone-derived films was also quantified (Figure 7a). The thermal conductivity of ALD alumina has been shown to vary from 1.3 to 2.6 W/(m·K) with thicknesses ranging from 10 to 200 nm.[22] All of the capped alucone samples, regardless of processing conditions, had thermal conductivity values (0.5−1.1 W/(m·K)) lower than those reported for ALD alumina. The decreased thermal conductivity for the UV-cured alucone sample at 150 and 250 °C relative to the as-deposited state likely corresponds to the removal of organics and porosity formation. The subsequent increase in thermal conductivity after annealing at 350 °C is driven by densification. The alucone samples annealed at 250 and 350 °C in the absence of UV show similar trends in thermal conductivity values when compared to UV-cured alucone, with the 150 °C-annealed sample being the only exception. Since the free volume inside alucone may increase with the removal of organics and the formation of porosity, the thermal conductivity is expected to decrease with increasing porosity.[75] The removal of organics and pore formation that occurs at lower temperatures (150 and 250 °C) decreases the thermal conductivity, whereas further structural collapse and densification at 350 °C leads to increases in the thermal conductivity. Thus, from just thermal conductivity data, the highest porosity is expected for the 150 and 250 °C-processed films.

The presence of open porosity was examined using ellipsometric porosity (Figure 7b). The adsorption isotherms were initially measured using water and toluene, which showed irreversible hysteresis indicating absorption. Irreversible hysteresis indicates the presence of a wide range of interconnected pore sizes, which makes the analysis of pore size distribution difficult.[76−78] When isopropanol (IPA) was

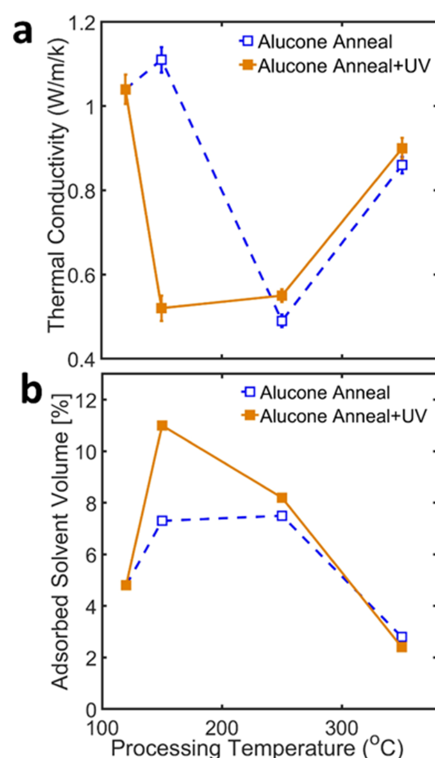

Figure 7. (a) Thermal conductivity vs annealing temperature of alucone films (deposited at 120 °C) capped with 10 ALD alumina cycles and (b) ellipsometric porosimetry solvent absorption vs annealing temperature of as-deposited and processed uncapped alucones.

used as a probe, the hysteresis behavior was reversible and hence IPA was used to probe the porosity of all of the films. The adsorbed solvent volume initially increased when processed at 150 °C and ultimately decreased after processing at 350 °C. This trend may be due to the initial formation of accessible pores and the subsequent collapse of those pores at higher temperatures. This trend in adsorbed volume also coincides with the decreasing thickness and increasing density of alucone samples with increasing temperature as seen by XRR and RBS/NRA. These data also support the formation of the most porous structures at the intermediate temperatures investigated and a collapse or closure of pores at higher temperatures and follow the trends observed in thermal conductivity.

The indentation modulus of the alucone films was measured as the mechanical stability of films is highly important for applications in electronics and is expected to be correlated with porosity (Figure 8), whereas the indentation modulus of the alucone films remained low (30−40 GPa) relative to known values for alumina (∼200 GPa)[37] and did not change substantially until the 250 °C anneal temperature. The increase in modulus at 350 °C is coincident with the increase in density and decrease in thickness. The indentation modulus of the as-deposited and 350 °C-annealed alucone samples is similar to that of as-deposited alucone (21 ± 8 GPa) and 3:1 Al_2O_3/alucone (85 ± 8 GPa) alloy from the literature, respectively.[37]

Since the dry etch rate of dielectric films is important for IC processing and also indicative of structural differences among samples, the etch rate of the 10 ALD cycle-capped alucone, uncapped alucone, and alumina was quantified in CF_4/O_2

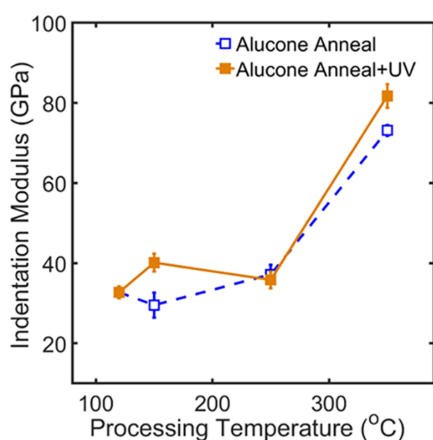

Figure 8. Indentation modulus vs annealing temperature of as-deposited (120 °C) and annealed alucone films, both with and without UV.

plasma (Figure 9). The etch rates of the as-deposited and thermally processed alucone films were larger than those of the

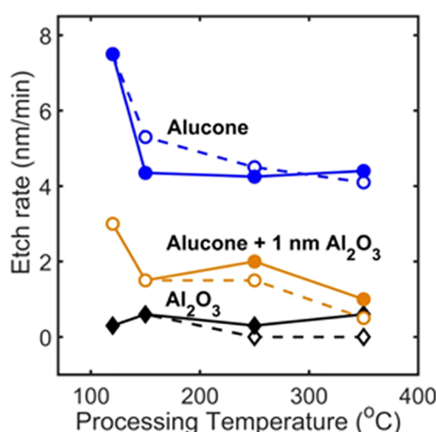

Figure 9. CF_4/O_2 plasma etch rate of as-deposited alucone (deposited at 120 °C), 10-cycle-capped alucone, and alumina after annealing or annealing in UV.

alucone films with a 1 nm alumina barrier and alumina control films. The etch rate of the alucone films decreased significantly from 8 to 4 nm/min after annealing at 150 °C and then remained constant, whereas the etch rate of as-deposited and thermally processed alumina films was 0−1 nm/min. The etch rate of the alucone films with ALD barrier layers decreased from 3.5 to 1 nm/min after annealing at 350 °C. Generally, the etch rate is shown to decrease with increasing alumina content (e.g., pure alumina films and alumina-capped alucone films) and to decrease with increasing processing temperature, presumably due to a densification of the film and outer surface layers. The UV curing had a minimal impact on the dry etch rates of all of the films. As discussed previously, the 1 nm alumina barrier layer may also form new alumina domains inside the film. These increased alumina-like domains may be responsible for the decrease in the dry etch rate of the capped films.

Considering the overall impact on annealing of the alucone films, we believe that this work shows the promise of MLD films as precursors for porous and/or low-k thin films. Generally, thermal processing has been shown to remove organic components and introduce porosity. At high enough temperatures, structural collapse and increases in density and dielectric constant were observed. The structural collapse observed as a thickness decrease is not unexpected due to the lack of continuous inorganic framework around the organic ethylene glycol units. However, due to the large variety of inorganic ALD precursors and potential organic MLD precursors, a large platform of precursor combinations is available for the formation of porous MLD-derived thin films. This work also shows the promise of using thin capping layers on MLD and porous thin films to prevent the uptake of an atmospheric component such as water.

■ CONCLUSIONS

The thermal and UV processing of hybrid MLD alucone films are shown to result in porous films with smaller k values than control ALD alumina samples. The alucone films exhibit a decrease in film thickness with increasing thermal processing temperature while maintaining a lower density than ALD alumina films. The decrease in thickness is coincident with a decrease in the OH and CH_2 stretching regions in FTIR spectra. RBS/NRA indicated a continual removal of H and C from the films when processed from the as-deposited state to 350 °C. Thermal conductivity and ellipsometric porosimetry also indicated porosity within the films that reaches a maximum at 150 and 250 °C process temperatures and then decreases with annealing at 350 °C, presumably due to collapse of the remaining inorganic structure, which is further supported by similar trends in the elastic modulus at the highest processing temperature. This study provides evidence that the thermal processing of hybrid MLD films provides an approach to porous solids similar to polymer or other organic templates used to make porous solids.[34,42,79] Thus, similar approaches may find use in porous films for electronics, catalysis, separations, and sensors.

■ ASSOCIATED CONTENT

Supporting Information

The Supporting Information is available free of charge at https://pubs.acs.org/doi/10.1021/acs.chemmater.2c03107.

Schematic of alucone growth; MLD saturation curves; *ex-situ* XRR data of alucone and alumina; raw *in-situ* XRR data of alucone and alumina with fits; tables of density, thickness, and surface roughness of alucone and alumina; SEM images of alucone; MOSCAP device structures; and ellipsometric porosimetry data showing refractive index @ 632 nm vs time and relative pressure (P/P_0) vs time (PDF)

■ AUTHOR INFORMATION

Corresponding Author

Nicholas C. Strandwitz − *Department of Materials Science and Engineering, Lehigh University, Bethlehem, Pennsylvania 18015, United States;* orcid.org/0000-0001-6159-9430; Email: strand@lehigh.edu

Authors

Vamseedhara Vemuri − *Department of Materials Science and Engineering, Lehigh University, Bethlehem, Pennsylvania 18015, United States;* orcid.org/0000-0001-5284-1803

https://doi.org/10.1021/acs.chemmater.2c03107
Chem. Mater. 2023, 35, 1916−1925

Sean W. King − *Logic Technology Development, Intel Corporation, Hillsboro, Oregon 97124, United States;* orcid.org/0000-0001-5400-7679
William A. Lanford − *Department of Physics, University at Albany, Albany, New York 12222, United States*
John T. Gaskins − *Laser Thermal Analysis, Inc., Charlottesville, Virginia 22902, United States*
Patrick Edward Hopkins − *Department of Mechanical and Aerospace Engineering, University of Virginia, Charlottesville, Virginia 22904, United States*
Jeremy Van Derslice − *J.A. Woollam, Lincoln, Nebraska 68508, United States*
Han Li − *CQN Labs, Intel Corporation, Hillsboro, Oregon 97124, United States*

Complete contact information is available at:
https://pubs.acs.org/10.1021/acs.chemmater.2c03107

Notes

The authors declare no competing financial interest.

■ ACKNOWLEDGMENTS

The authors would like to thank Intel Corporation for funding and Md. Istiaque Chowdhary for performing SEM imaging of the alucone films. P.E.H. appreciates the support from the Army Research Office, Grant Number W911NF-16-1-0406. The authors would also like to thank Dr. Andy Antonelli for having discussions about the UV cure chamber and Nolan Sornson for helping them design and build the chamber.

■ REFERENCES

(1) Volksen, W.; Miller, R. D.; Dubois, G. Low Dielectric Constant Materials. *Chem. Rev.* **2010**, *110*, 56−110.
(2) Andricacos, P. C.; Uzoh, C.; Dukovic, J. O.; Horkans, J.; Deligianni, H. Damascene Copper Electroplating for Chip Interconnections. *IBM J. Res. Dev.* **1998**, *42*, 567−573.
(3) King, S. W. Dielectric Barrier, Etch Stop, and Metal Capping Materials for State of the Art and beyond Metal Interconnects. *ECS J. Solid State Sci. Technol.* **2015**, *4*, N3029−N3047.
(4) Shamiryan, D.; Abell, T.; Iacopi, F.; Maex, K. Low-k Dielectric Materials. *Mater. Today* **2004**, *7*, 34−39.
(5) Tambat, A.; Lin, H. Y.; Subbarayan, G.; Jung, D. Y.; Sammakia, B. Simulations of Damage, Crack Initiation, and Propagation in Interlayer Dielectric Structures: Understanding Assembly-Induced Fracture in Dies. *IEEE Trans. Device Mater. Reliab.* **2012**, *12*, 241−254.
(6) Rhee, S.-H.; Du, Y.; Ho, P. S. Thermal Stress Characteristics of Cu/Oxide and Cu/Low-k Submicron Interconnect Structures. *J. Appl. Phys.* **2003**, *93*, 3926.
(7) Wang, G.; Ho, P. S.; Groothuis, S. Chip-Packaging Interaction: A Critical Concern for Cu/Low k Packaging. *Microelectron. Reliab.* **2005**, *45*, 1079−1093.
(8) Luo, Y.; Subbarayan, G. A Study of Multiple Singularities in Multi-Material Wedges and Their Use in Analysis of Microelectronic Interconnect Structures. *Eng. Fract. Mech.* **2007**, *74*, 416−430.
(9) Lanckmans, F.; Gray, W. D.; Brijs, B.; Maex, K. A Comparative Study of Copper Drift Diffusion in Plasma Deposited A-SiC:H and Silicon Nitride. *Microelectron. Eng.* **2001**, *55*, 329−335.
(10) Shieh, J.-M.; Tsai, K.-C.; Dai, B.-T. Low Hydrogen Content in Trimethylsilane-Based Dielectric Barriers Deposited by Inductively Coupled Plasma. *Appl. Phys. Lett.* **2002**, *81*, 1294.
(11) Shieh, J.-M.; Tsai, K.-C.; Dai, B.-T. Ultralow Copper Drift in Inductively Coupled Plasma Silicon Carbide Dielectrics. *Appl. Phys. Lett.* **2003**, *82*, 1914.
(12) Chiang, C.-C.; Wu, Z.-C.; Wu, W.-H.; Chen, M.-C.; Ko, C.-C.; Chen, H.-P.; Jang, S.-M.; Yu, C.-H.; Liang, M.-S. Physical and Barrier Properties of Plasma Enhanced Chemical Vapor Deposition α-SiC:N:H Films. *Jpn. J. Appl. Phys.* **2003**, *42*, 4489.
(13) Charles-Alfred, C.; Jousseaume, V. A-SiC:H Low-k Deposition as Copper Diffusion Barrier Layer in Advanced Microelectronic Interconnections. *Surf. Coat. Technol.* **2007**, *201*, 9260−9263.
(14) King, S. W.; Bielefeld, J.; Xu, G.; Lanford, W. A.; Matsuda, Y.; Dauskardt, R. H.; Kim, N.; Hondongwa, D.; Olasov, L.; Daly, B.; et al. Influence of Network Bond Percolation on the Thermal, Mechanical, Electrical and Optical Properties of High and Low-k a-SiC:H Thin Films. *J. Non-Cryst. Solids* **2013**, *379*, 67−79.
(15) Chiang, C.-C.; Chen, M.-C.; Ko, C.-C.; Jang, S.-M.; Yu, C.-H.; Liang, M.-S. Physical and Barrier Properties of Plasma-Enhanced Chemical Vapor Deposited α-SiCN:H Films with Different Hydrogen Contents. *Jpn. J. Appl. Phys.* **2003**, *42*, 5246.
(16) Fainer, N.; Rumyantsev, Y.; Kosinova, M.; Maximovski, E.; Kesler, V.; Kirienko, V.; Kuznetsov, F. Low-k Dielectrics on Base of Silicon Carbon Nitride Films. *Surf. Coat. Technol.* **2007**, *201*, 9269−9274.
(17) Mallikarjunan, A.; Johnson, A. D.; Matz, L.; Vrtis, R. N.; Derecskei-Kovacs, A.; Jiang, X.; Xiao, M. Silicon Precursor Development for Advanced Dielectric Barriers for VLSI Technology. *Microelectron. Eng.* **2012**, *92*, 83−85.
(18) Tu, H.-E.; Chen, Y.-H.; Leu, J. Low-k SiCxNy Films Prepared by Plasma-Enhanced Chemical Vapor Deposition Using 1,3,5-Trimethyl-1,3,5-Trivinylcyclotrisilazane Precursor. *J. Electrochem. Soc.* **2012**, *159*, G56.
(19) King, S. W. Plasma Enhanced Atomic Layer Deposition of SiNx:H and SiO2. *J. Vac. Sci. Technol. A* **2011**, *29*, No. 041501.
(20) Parsons, G. N.; Souk, J. H.; Batey, J. Low Hydrogen Content Stoichiometric Silicon Nitride Films Deposited by Plasma-enhanced Chemical Vapor Deposition. *J. Appl. Phys.* **1991**, *70*, 1553.
(21) Dupont, G.; Caquineau, H.; Despax, B.; Berjoan, R.; Dollet, A. Structural Properties of N-Rich a-Si - N:H Films with a Low Electron-Trapping Rate. *J. Phys. D: Appl. Phys.* **1997**, *30*, 1064.
(22) Scott, E. A.; Gaskins, J. T.; King, S. W.; Hopkins, P. E. Thermal Conductivity and Thermal Boundary Resistance of Atomic Layer Deposited High- k Dielectric Aluminum Oxide, Hafnium Oxide, and Titanium Oxide Thin Films on Silicon. *APL Mater.* **2018**, *6*, No. 058302.
(23) Luo, Z.; Liu, H.; Spann, B. T.; Feng, Y.; Ye, P.; Chen, Y. P.; Xu, X. Measurement of In-Plane Thermal Conductivity of Ultrathin Films Using Micro-Raman Spectroscopy. *Nanoscale Microscale Thermophys. Eng.* **2014**, *18*, 183−193.
(24) Gorham, C. S.; Gaskins, J. T.; Parsons, G. N.; Losego, M. D.; Hopkins, P. E. Density Dependence of the Room Temperature Thermal Conductivity of Atomic Layer Deposition-Grown Amorphous Alumina (Al2O3). *Appl. Phys. Lett.* **2014**, *104*, No. 253107.
(25) Tripp, M. K.; Stampfer, C.; Miller, D. C.; Helbling, T.; Herrmann, C. F.; Hierold, C.; Gall, K.; George, S. M.; Bright, V. M. The Mechanical Properties of Atomic Layer Deposited Alumina for Use in Micro- and Nano-Electromechanical Systems. *Sens. Actuators, A* **2006**, *130*−*131*, 419−429.
(26) Higashi, G. S.; Fleming, C. G. Sequential Surface Chemical Reaction Limited Growth of High Quality Al2O3 Dielectrics. *Appl. Phys. Lett.* **1989**, *55*, 1963.
(27) Yang, W. S.; Kim, Y. K.; Yang, S. Y.; Choi, J. H.; Park, H. S.; Lee, S. I.; Yoo, J. B. Effect of SiO2 Intermediate Layer on Al2O3/SiO2/N+-Poly Si Interface Deposited Using Atomic Layer Deposition (ALD) for Deep Submicron Device Applications. *Surf. Coat. Technol.* **2000**, *131*, 79−83.
(28) Kukli, K.; Ritala, M.; Leskelä, M.; Jokinen, J. Atomic Layer Epitaxy Growth of Aluminum Oxide Thin Films from a Novel Al(CH3)2Cl Precursor and H2O. *J. Vac. Sci. Technol. A* **1997**, *15*, 2214.
(29) Fan, J.-F.; Sugioka, K. S. K.; Toyoda, K. T. K. Low-Temperature Growth of Thin Films of Al2O3 by Sequential Surface Chemical Reaction of Trimethylaluminum and H2O2. *Jpn. J. Appl. Phys.* **1991**, *30*, L1139.

(30) Acharya, J.; Wilt, J.; Liu, B.; Wu, J. Probing the Dielectric Properties of Ultrathin Al/Al2O3/Al Trilayers Fabricated Using in Situ Sputtering and Atomic Layer Deposition. *ACS Appl. Mater. Interfaces* **2018**, *10*, 3112−3120.
(31) Verdonck, P.; De Roest, D.; Kaneko, S.; Caluwaerts, R.; Tsuji, N.; Matsushita, K.; Kemeling, N.; Travaly, Y.; Sprey, H.; Schaekers, M.; Beyer, G. Characterization and Optimization of Porogen-Based PECVD Deposited Extreme Low-k Materials as a Function of UV-Cure Time. *Surf. Coat. Technol.* **2007**, *201*, 9264−9268.
(32) Ming, Z.; Beichao, Z. Preparation of Porous Ultra Low k Films Using Different Sacrificial Porogen Precursors for 28 NM Technological Node. *Mater. Sci. Semicond. Process.* **2015**, *36*, 170−178.
(33) Zhao, D.; Feng, J.; Huo, Q.; Melosh, N.; Fredrickson, G. H.; Chmelka, B. F.; Stucky, G. D. Triblock Copolymer Syntheses of Mesoporous Silica with Periodic 50 to 300 Angstrom Pores. *Science* **1998**, *279*, 548−552.
(34) Huo, Q.; Margolese, D. I.; Ciesla, U.; Feng, P.; Gier, T. E.; Sieger, P.; Leon, R.; Petroff, P. M.; Schüth, F.; Stucky, G. D. Generalized Synthesis of Periodic Surfactant/Inorganic Composite Materials. *Nature* **1994**, *368*, 317−321.
(35) Liang, X.; Yu, M.; Li, J.; Jiang, Y.-B.; Weimer, A. W. Ultra-Thin Microporous−Mesoporous Metal Oxide Films Prepared by Molecular Layer Deposition (MLD). *Chem. Commun.* **2009**, *0*, 7140.
(36) Dameron, A. A.; Seghete, D.; Burton, B. B.; Davidson, S. D.; Cavanagh, A. S.; Bertrand, J. A.; George, S. M. Molecular Layer Deposition of Alucone Polymer Films Using Trimethylaluminum and Ethylene Glycol. *Chem. Mater.* **2008**, *20*, 3315−3326.
(37) Lee, B. H.; Yoon, B.; Anderson, V. R.; George, S. M. Alucone Alloys with Tunable Properties Using Alucone Molecular Layer Deposition and Al2O3 Atomic Layer Deposition. *J. Phys. Chem. C* **2012**, *116*, 3250−3257.
(38) Dumont, J. W.; George, S. M. Pyrolysis of Alucone Molecular Layer Deposition Films Studied Using in Situ Transmission Fourier Transform Infrared Spectroscopy. *J. Phys. Chem. C* **2015**, *119*, 14603−14612.
(39) Ghazaryan, L.; Kley, E.-B.; Tünnermann, A.; Szeghalmi, A. V. Stability and Annealing of Alucones and Alucone Alloys. *J. Vac. Sci. Technol. A* **2013**, *31*, No. 01A149.
(40) Van De Kerckhove, K.; Barr, M. K. S.; Santinacci, L.; Vereecken, P. M.; Dendooven, J.; Detavernier, C. The Transformation Behaviour of "Alucones", Deposited by Molecular Layer Deposition, in Nanoporous Al2O3 Layers. *Dalton Trans.* **2018**, *47*, 5860−5870.
(41) Liang, X.; Evanko, B. W.; Izar, A.; King, D. M.; Jiang, Y. B.; Weimer, A. W. Ultrathin Highly Porous Alumina Films Prepared by Alucone ABC Molecular Layer Deposition (MLD). *Microporous Mesoporous Mater.* **2013**, *168*, 178−182.
(42) Liang, X.; Li, J.; Yu, M.; McMurray, C. N.; Falconer, J. L.; Weimer, A. W. Stabilization of Supported Metal Nanoparticles Using an Ultrathin Porous Shell. *ACS Catal.* **2011**, *1*, 1162−1165.
(43) Perrotta, A.; Poodt, P.; Van Den Bruele, F. J.; Kessels, W. M. M.; Creatore, M. Characterization of Nano-Porosity in Molecular Layer Deposited Films. *Dalton Trans.* **2018**, *47*, 7649−7655.
(44) Che, M. L.; Teng, J. Y.; Lai, P. C.; Leu, J. Moisture Uptake and Dielectric Property of Methylsilsesquioxane/High-Temperature Porogen Hybrids and Porous Low-k Films. *J. Mater. Res.* **2011**, *26*, 2987−2995.
(45) Tagami, M.; Ogino, A.; Miyajima, H.; Shobha, H.; Baumann, F. H.; Ito, F.; Spooner, T. Moisture Uptake Impact on Damage Layer of Porous Low-k Film in 80nm-Pitched Cu Interconnects. *ECS Trans.* **2011**, *41*, 405.
(46) Michelon, J.; Hoofman, R. J. O. M. Moisture Influence on Porous Low-k Reliability. *IEEE Trans. Device Mater. Reliab.* **2006**, *6*, 169−174.
(47) Elam, J. W.; Groner, M. D.; George, S. M. Viscous Flow Reactor with Quartz Crystal Microbalance for Thin Film Growth by Atomic Layer Deposition. *Rev. Sci. Instrum.* **2002**, *73*, 2981.
(48) Ju, L.; Vemuri, V.; Strandwitz, N. C. Quartz Crystal Microbalance Study of Precursor Diffusion during Molecular Layer Deposition Using Cyclic Azasilane, Maleic Anhydride, and Water. *J. Vac. Sci. Technol. A* **2019**, *37*, No. 030909.
(49) Kern, W. Evolution of Silicon Wafer Cleaning Technology. *Proc. Electrochem. Soc.* **1990**, *90*, 3−19.
(50) Lanford, W. A.; Parenti, M.; Nordell, B. J.; Paquette, M. M.; Caruso, A. N.; Mäntymäki, M.; Hämäläinen, J.; Ritala, M.; Klepper, K. B.; Miikkulainen, V.; et al. Nuclear Reaction Analysis for H, Li, Be, B, C, N, O and F with an RBS Check. *Nucl. Instruments Methods Phys. Res. Sect. B* **2016**, *371*, 211−215.
(51) Braun, J. L.; Olson, D. H.; Gaskins, J. T.; Hopkins, P. E. A Steady-State Thermoreflectance Method to Measure Thermal Conductivity. *Rev. Sci. Instrum.* **2019**, *90*, No. 024905.
(52) Tian, X.; Goh, T. W.; Vandenberg, O.; Vanderslice, J.; Da Silva, T. F.; Naab, F.; Hay, J. L.; Chang, J. J.; Yuan, B.; Peiris, F. C.; et al. Self-Regulated Porosity and Reactivity in Mesoporous Heterogeneous Catalysts Using Colloidal Nanocrystals. *J. Phys. Chem. C* **2019**, *123*, 18410−18416.
(53) Gaskins, J. T.; Hopkins, P. E.; Merrill, D. R.; Bauers, S. R.; Hadland, E.; Johnson, D. C.; Koh, D.; Yum, J. H.; Banerjee, S.; Nordell, B. J.; et al. Review—Investigation and Review of the Thermal, Mechanical, Electrical, Optical, and Structural Properties of Atomic Layer Deposited High- k Dielectrics: Beryllium Oxide, Aluminum Oxide, Hafnium Oxide, and Aluminum Nitride. *ECS J. Solid State Sci. Technol.* **2017**, *6*, N189−N208.
(54) Fu, P.; Hu, S.; Xiang, J.; Li, P.; Huang, D.; Jiang, L.; Zhang, A.; Zhang, J. FTIR Study of Pyrolysis Products Evolving from Typical Agricultural Residues. *J. Anal. Appl. Pyrolysis* **2010**, *88*, 117−123.
(55) Fu, P.; Hu, S.; Xiang, J.; Sun, L.; Yang, T.; Zhang, A.; Zhang, J. Mechanism Study of Rice Straw Pyrolysis by Fourier Transform Infrared Technique. *Chin. J. Chem. Eng.* **2009**, *17*, 522−529.
(56) Ōtani, S. On the Carbon Fiber from the Molten Pyrolysis Products. *Carbon* **1965**, *3*, 31−38.
(57) Lewis, I. C. Chemistry of Carbonization. *Carbon* **1982**, *20*, 519−529.
(58) George, C.; Littlewood, P.; Stair, P. C. Understanding Pore Formation in ALD Alumina Overcoats. *ACS Appl. Mater. Interfaces* **2020**, *12*, 20331−20343.
(59) Kao, K.-C.; Chang, W.-Y.; Chang, Y.-M.; Leu, J.; Cheng, Y.-L. Effect of UV Curing Time on Physical and Electrical Properties and Reliability of Low Dielectric Constant Materials. *J. Vac. Sci. Technol. A* **2014**, *32*, No. 061514.
(60) Smith, R. S.; Tsui, T.; Ho, P. S. Analysis of Ultraviolet Curing Effect on the Dielectric Constant and Molecular Structure of a Porous Dielectric Film. *J. Electron. Mater.* **2010**, *39*, 2337−2345.
(61) Eslava, S.; Eymery, G.; Marsik, P.; Iacopi, F.; Kirschhock, C. E. A.; Maex, K.; Martens, J. A.; Baklanov, M. R. Optical Property Changes in Low-k Films upon Ultraviolet-Assisted Curing. *J. Electrochem. Soc.* **2008**, *155*, G115.
(62) Jobson, E.; Baiker, A.; Wokaun, A. Interaction of Ethylene Glycol with Alumina Supported Copper —an FTIR Study. *Ber. Bunsenges. Phys. Chem.* **1989**, *93*, 64−70.
(63) Colthup, N. B.; Daly, L. H.; Wiberley, S. E. *Introduction to Infrared and Raman Spectroscopy*; Elsevier, 1990; p 547.
(64) Makgoba, N. P.; Sakuneka, T. M.; Koortzen, J. G.; Van Schalkwyk, C.; Botha, J. M.; Nicolaides, C. P. Silication of γ-Alumina Catalyst during the Dehydration of Linear Primary Alcohols. *Appl. Catal., A* **2006**, *297*, 145−150.
(65) Colthup, N. B.; Daly, L. H.; Wiberley, S. E.Ethers, Alcohols, and Phenols. In *Introduction to Infrared and Raman Spectroscopy*; Elsevier, 1975; pp 311−320.
(66) Fisher, G. L.; Walker, A. V.; Hooper, A. E.; Tighe, T. B.; Bahnck, K. B.; Skriba, H. T.; Reinard, M. D.; Haynie, B. C.; Opila, R. L.; Winograd, N.; Allara, D. L. Bond Insertion, Complexation, and Penetration Pathways of Vapor-Deposited Aluminum Atoms with HO- and CH3O-Terminated Organic Monolayers. *J. Am. Chem. Soc.* **2002**, *124*, 5528−5541.
(67) Liu, H.; Bertolet, D. C.; Rogers, J. W. Reactions of Trimethylaluminum and Ammonia on Alumina at 600 K — Surface

Chemical Aspects of AlN Thin Film Growth. *Surf. Sci.* **1995**, *340*, 88–100.
(68) Frank, M.; Wolter, K.; Magg, N.; Heemeier, M.; Kühnemuth, R.; Bäumer, M.; Freund, H. J. Phonons of Clean and Metal-Modified Oxide Films: An Infrared and HREELS Study. *Surf. Sci.* **2001**, *492*, 270–284.
(69) Rochat, N.; Troussier, A.; Hoang, A.; Vinet, F. Multiple Internal Reflection Spectroscopy for Quantitative Infrared Analysis of Thin-Film Surface Coating for Biological Environment. *Mater. Sci. Eng. C* **2003**, *23*, 99–103.
(70) Davis, K. M.; Tomozawa, M. Water Diffusion into Silica Glass: Structural Changes in Silica Glass and Their Effect on Water Solubility and Diffusivity. *J. Non-Cryst. Solids* **1995**, *185*, 203–220.
(71) Feijoó, D.; Chabal, Y. J.; Christman, S. B. Silicon Wafer Bonding Studied by Infrared Absorption Spectroscopy. *Appl. Phys. Lett.* **1994**, *65*, 2548.
(72) Jarvis, K. L.; Evans, P. J. Growth of Thin Barrier Films on Flexible Polymer Substrates by Atomic Layer Deposition. *Thin Solid Films* **2017**, *624*, 111–135.
(73) Jain, H.; Poodt, P. About the Importance of Purge Time in Molecular Layer Deposition of Alucone Films. *Dalton Trans.* **2021**, *50*, 5807–5818.
(74) Kolb, J.; Minamitani, Y.; Xiao, S.; Lu, X.; Laroussi, M.; Joshi, R. P.; Schoenbach, K. H.; Schamiloglu, E.; Gaudet, J.In *The Permittivity of Water under High Dielectric Stress*, Digest of Technical Papers, IEEE International Pulsed Power Conference, 2007; pp 1266–1269.
(75) Saini, S.; Mele, P.; Oyake, T.; Shiomi, J.; Niemelä, J. P.; Karppinen, M.; Miyazaki, K.; Li, C.; Kawaharamura, T.; Ichinose, A.; Molina-Luna, L. Porosity-Tuned Thermal Conductivity in Thermoelectric Al-Doped ZnO Thin Films Grown by Mist-Chemical Vapor Deposition. *Thin Solid Films* **2019**, *685*, 180–185.
(76) Rouessac, V.; Coustel, R.; Bosc, F.; Durand, J.; Ayral, A. Characterisation of Mesostructured TiO2 Thin Layers by Ellipsometric Porosimetry. *Thin Solid Films* **2006**, *495*, 232–236.
(77) Borrás, A.; Sánchez-Valencia, J. R.; Garrido-Molinero, J.; Barranco, A.; González-Elipe, A. R. Porosity and Microstructure of Plasma Deposited TiO2 Thin Films. *Microporous Mesoporous Mater.* **2009**, *118*, 314–324.
(78) Alvarez-Herrero, A.; Ramos, G.; Del Monte, F.; Bernabeu, E.; Levy, D. Water Adsorption in Porous TiO2–SiO2 Sol–Gel Films Analyzed by Spectroscopic Ellipsometry. *Thin Solid Films* **2004**, *455–456*, 356–360.
(79) Bagshaw, S. A.; Prouzet, E.; Pinnavaia, T. J. Templating of Mesoporous Molecular Sieves by Nonionic Polyethylene Oxide Surfactants. *Science* **1995**, *269*, 1242–1244.

Recommended by ACS

Inhibitor-Free Area-Selective Atomic Layer Deposition with Feature Size Down to Nearly 10 nm

Chun-Yi Chou, Miin-Jang Chen, *et al.*

JANUARY 30, 2023
CHEMISTRY OF MATERIALS

Impact of the Density and Oxygen Concentration of Initial Amorphous Carbon on Layer Exchange of Multilayer Graphene

Hiromasa Murata, Masayoshi Nagao, *et al.*

NOVEMBER 14, 2022
CRYSTAL GROWTH & DESIGN

Thermal Atomic Layer Etching of Al_2O_3 Using Sequential HF and BCl_3 Exposures: Evidence for Combined Ligand-Exchange and Conversion Mechanisms

Austin M. Cano, Steven M. George, *et al.*

JULY 11, 2022
CHEMISTRY OF MATERIALS

High-Quality AlN Grown by a Combination of Substrate Pretreatment and Periodic Growth Mode Control

Shengyuan Dong, Zhongming Zeng, *et al.*

MAY 31, 2023
CRYSTAL GROWTH & DESIGN

Get More Suggestions >

https://doi.org/10.1021/acs.chemmater.2c03107
Chem. Mater. 2023, 35, 1916–1925